Cosmic-Ray Bounds on Lepton-Flavor-Violating Dark-Matter Decays*

A thesis submitted in partial fulfillment of the requirement
for the degree of Bachelor of Science with Honors in
Physics from the College of William & Mary in Virginia,

by

Ari J. Cukierman

Accepted for ___ Honors ___

(Honors)

Advisor: Christopher D. Carone
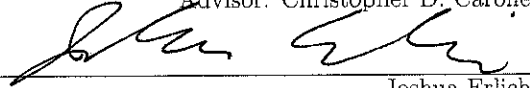
Joshua Erlich

Gexin Yu

Henry Krakauer

Williamsburg, Virginia
April 2012

Cosmic-Ray Bounds on Lepton-Flavor-Violating Dark-Matter Decays*

Ari J. Cukierman

Abstract

We consider possible leptonic three-body decays of spin-1/2 charge-asymmetric dark matter. Assuming a general Dirac structure for the four-fermion contact interactions of interest, we study the cosmic-ray electron and positron spectra and show that good fits to the current data can be obtained for both charged-lepton-flavor-conserving and flavor-violating decay channels. We find that different choices for the Dirac structure of the underlying decay operator can be significantly compensated by different choices for the dark-matter mass and lifetime. The decay modes we consider provide differing predictions for the cosmic-ray positron fraction at energies higher than those currently probed at the PAMELA experiment; these predictions might be tested at cosmic-ray detectors like AMS-02. Additionally, we consider the constraints imposed on these decays by neutrino and gamma-ray observatories.

Acknowledgements

Contents

List of Figures

Chapter 1

Introduction

Cosmic rays have been studied extensively at various earth-, balloon- and satellite-based experiments. Recently, the PAMELA satellite has observed an unexpected rise in the cosmic-ray positron fraction from approximately 7 to $100\,\text{GeV}$ [1]. This feature is not explained by the expected background from the secondary production of cosmic-rays positrons. Moreover, observations of the total flux of electrons and positrons by Fermi-LAT [2] and H.E.S.S. [3] also show an excess over the predicted background, up to an energy of $\sim 1\,\text{TeV}$. The presence of nearby pulsars could provide an astrophysical explanation for these observations [4, 5]. Nevertheless, more exotic scenarios remain possible. The annihilation of dark matter in the galactic halo to electrons and positrons provides one such possibility, though generic annihilation cross sections must be enhanced by a large boost factor in order to describe the data [6, 7]. Alternatively, the excess could be explained by a TeV-scale decaying dark matter candidate. (For a review, see, for example, Ref. [9].) In this scenario, fits to the cosmic-ray data indicate that the dark matter must decay primarily to leptons with a lifetime of $\mathcal{O}(10^{26})\,\text{s}$.

While the thermal freeze-out of weakly-interacting, electroweak-scale dark matter can naturally lead to the desired relic density, this is not the only possible frame-

work that can account for the present dark matter abundance. Recently proposed asymmetric dark-matter models relate the baryon- or lepton-number densities to the dark-matter number density motivated by the fact that these quantities are not wildly dissimilar [10, 11, 12, 13]. TeV-scale asymmetric dark-matter models have been constructed, for example, in Refs. [11, 12, 13]. The asymmetry between dark-matter particles and antiparticles can lead to differences in the primary cosmic-ray spectra of electrons and positrons with potentially measurable consequences [15]. Evidence for such charge-asymmetric dark-matter decays would disfavor the pulsar explanation of the $e^{\pm}$ excess [15]. In addition, charge-asymmetric dark-matter decays may allow one to discern whether dark-matter decays are lepton-flavor-violating [16]. For example, the cosmic-ray spectra that one expects if dark matter decays symmetrically to $e^{+}\mu^{-}$ and $e^{-}\mu^{+}$ are indistinguishable from those obtained by assuming flavor-conserving decays to $e^{+}e^{-}$ and $\mu^{+}\mu^{-}$ with equal branching fractions; the same is not true if the dark matter decays asymmetrically to $e^{+}\mu^{-}$ alone, 100% of the time.

References [15] and [16] study the cosmic-ray $e^{\pm}$ spectra assuming a number of two-body charge-asymmetric dark-matter decays, with the latter work focusing on lepton-flavor-violating modes. In this thesis, we extend this body of work to charge-asymmetric three-body decays and, in particular, to modes that violate lepton flavor. We assume a spin-1/2 dark-matter candidate that decays via four-fermion contact interactions to two charged leptons and a light, stable neutral particle. For the present purposes, the latter could either be a standard-model neutrino or a lighter dark-matter component. Four-fermion interactions have a long history in the development of the weak interactions, and one can easily imagine that dark-matter decays could be the consequence of operators of this form, generated by higher-scale physics. Moreover, the possible presence of a neutrino in the primary decay may lead to interesting signals at neutrino telescopes [17]. Unlike the two-body decays already considered in the literature, the precise energy distribution of the decay products is affected by

the Dirac matrix structure of these contact interactions, which is not known (unless a model is specified). By considering the most general possibilities, we show that different choices for the Dirac structure of the underlying decay operator can be substantially compensated by different choices for the dark-matter mass m_ψ and lifetime τ_ψ; while the best-fit values of these parameters change, the predicted spectra are not dramatically altered. On the other hand, we find that the flavor structure of the decay operator has a more significant effect. Assuming various lepton-flavor-conserving and flavor-violating decay modes, we compute the resulting cosmic-ray spectra, performing χ^2 fits to the data to determine the optimal dark-matter masses and lifetimes. Like Refs. [15, 16], we obtain predictions for these spectra at $e^\pm$ energies that are higher than those than can be probed accurately now. Future data from experiments like AMS-02 [18] may provide the opportunity to test these predictions, and evaluate them relative to other interpretations of the cosmic-ray positron excess.

Measurements of astrophysical neutrinos and gamma rays can also provide strong constraints on the decays considered in this thesis [17, 39]. We show that a null signal from IceCube/DeepCore after 5 years of running is enough to exclude several decays with a statistical significance of 2σ or more. On the other hand, IceCube measurements could yield a 5σ discovery for several decays within 5 years of running. Now, it is possible that dark-matter decays occur but are not entirely responsible for the $e^\pm$ excess observed by PAMELA and Fermi. In this case, it is still possible to exclude/detect other regions of the dark-matter mass-lifetime parameter space on the basis of the neutrino and gamma-ray fluxes. We have computed the regions which can be excluded with a statistical significance of 2σ or more and the regions which can be detected with a statistical significance of 5σ or more after 5 years of running. The Fermi LAT has also released measurements of the extragalactic gamma-ray background [39]. These data can be used to constrain dark-matter decays. We show that none of the three-body decays which are used to explain the $e^\pm$ excess is

in conflict with the Fermi data. However, as above, we can exclude other regions of the parameter space that may be relevant if dark-matter decays represent only a component of the $e^{\pm}$ excess. We compute the regions of the mass-lifetime parameter space which can be excluded by the Fermi LAT extragalactic gamma-ray background data with a statistical significance of 3σ or more.

Chapter 2

Cosmic-Ray Propagation

To compute the relevant cosmic-ray fluxes, one must take into account that electrons, positrons, neutrinos and gamma rays produced in dark-matter decays must propagate through galactic and/or intergalactic space before reaching the Earth. For the Milky Way Galaxy, we assume the spherically symmetric Navarro-Frenk-White (NFW) dark-matter-halo density profile [23]

$$\rho(r) = \frac{r_c}{r} \frac{\rho_0}{\left(1 + r/r_c\right)^2} \, , \tag{2.1}$$

where r denotes the distance from the center of the galaxy, $\rho_0 \simeq 0.26\,\mathrm{GeV/cm^3}$ and $r_c \simeq 20\,\mathrm{kpc}$.

2.1 Electron-Positron Propagation

The production rate of electrons/positrons per unit energy and per unit volume is given by

$$Q(E, r) = \frac{\rho(r)}{m_\psi} \left(\frac{1}{\tau_\psi} \frac{dN_{e^\pm}}{dE} \right) \, , \tag{2.2}$$

where m_ψ and τ_ψ are the dark-matter mass and lifetime, respectively, and $dN_{e^\pm}/dE$ is the energy spectrum of electrons/positrons produced in the dark-matter decay. Let

$f_{e^\pm}(E, \mathbf{r})$ be the number density of electrons/positrons per unit energy. Then $f_{e^\pm}$ satisfies the transport equation [24]

$$0 = K(E)\nabla^2 f_{e^\pm}(E, \mathbf{r}) + \frac{\partial}{\partial E}\left[b(E)f_{e^\pm}(E, \mathbf{r})\right] + Q(E, r). \qquad (2.3)$$

where $K(E)$ is the diffusion coefficient which accounts for propagation through the magnetic field of the galaxy and $b(E)$ accounts for energy losses due to synchotron radiation and inverse Compton scattering off of the interstellar radiation field. We assume the MED propagation model described in Ref. [25] for which

$$K(E) = 0.0112\epsilon^{0.70}\,\mathrm{kpc^2/Myr} \qquad (2.4)$$

and

$$b(E) = 10^{-16}\epsilon^2\,\mathrm{GeV/s}, \qquad (2.5)$$

where $\epsilon = E/\left(1\,\mathrm{GeV}\right)$. The diffusion zone is approximated as a cylinder with half-height $L = 4\,\mathrm{kpc}$ and radius $R = 20\,\mathrm{kpc}$. We require $f_{e^\pm}(E, \mathbf{r})$ to vanish at the boundary of this zone. The solution at the heliospheric boundary is then given by [26]

$$f_{e^\pm}(E) = \frac{1}{m_\psi \tau_\psi} \int\limits_0^{m_\psi} dE'\, G_{e^\pm}(E, E')\frac{dN_{e^\pm}(E')}{dE'}. \qquad (2.6)$$

The Green's function, $G_{e^\pm}(E, E')$, can be found in Ref. [26] in both an exact and an approximate form. The approximate form is

$$G_{e^\pm}(E, E') = \frac{10^{16}}{E^2}e^{a+b\left(E^{\delta-1}-E'^{\delta-1}\right)}\theta(E' - E), \qquad (2.7)$$

where $a = -1.0203$, $b = -1.4493$ and $\delta = 0.70$. This is good to better than $15 - 20\%$ over the whole range of energies.

The interstellar flux of electrons/positrons created in dark-matter decays is then

given by

$$\Phi_{e^\pm}^{\text{DM}}(E) = \frac{c}{4\pi} f_{e^\pm}(E), \tag{2.8}$$

where c is the speed of light.

For the background fluxes, we use the Model 0 proposed by the Fermi LAT collaboration [27, 28]:

$$\Phi_{e^-}^{\text{bkg}}(E) = \left(\frac{82.0\epsilon^{-0.28}}{1 + 0.224\epsilon^{2.93}} \right) \text{GeV}^{-1}\text{m}^{-2}\text{s}^{-1}\text{sr}^{-1} \tag{2.9}$$

and

$$\Phi_{e^+}^{\text{bkg}}(E) = \left(\frac{38.4\epsilon^{-4.78}}{1 + 0.0002\epsilon^{5.63}} + 24.0\epsilon^{-3.41} \right) \text{GeV}^{-1}\text{m}^{-2}\text{s}^{-1}\text{sr}^{-1}, \tag{2.10}$$

where, as before, $\epsilon = E/(1\,\text{GeV})$.

At the top of the Earth's atmosphere, these fluxes must be corrected to account for the effects of solar modulation [28]. The flux at the top of the atmosphere (TOA) is related to the interstellar (IS) flux by

$$\Phi_{e^\pm}^{\text{TOA}}(E_{\text{TOA}}) = \frac{E_{\text{TOA}}^2}{E_{\text{IS}}^2} \Phi_{e^\pm}^{\text{IS}}(E_{\text{IS}}), \tag{2.11}$$

where $E_{\text{IS}} = E_{\text{TOA}} + |e|\phi_F$ and $|e|\phi_F = 550\,\text{MeV}$.

The total electron-positron flux is given by

$$\Phi_e^{\text{tot}} = \Phi_{e^-}^{\text{DM}}(E) + \Phi_{e^+}^{\text{DM}}(E) + k\Phi_{e^-}^{\text{bkg}}(E) + \Phi_{e^+}^{\text{bkg}}(E), \tag{2.12}$$

where k is a free parameter which determines the normalization of the background electron flux. In our numerical analysis, the best-fit values of k never deviate by more than 2% from 0.84 and that fixing k at this value has a negligible effect on the goodness of fits and the predicted spectra. Therefore, we set $k = 0.84$ from this point

on. The positron fraction is given by

$$\text{PF}(E) = \frac{\Phi_{e^+}^{\text{DM}}(E) + \Phi_{e^+}^{\text{bkg}}(E)}{\Phi_e^{\text{tot}}}.$$ (2.13)

2.2 Neutrino Propagation

Define the line-of-sight integral

$$J(\Delta\Omega) = \frac{1}{\Delta\Omega} \int_{\Delta\Omega} d\Omega \int_{\text{l.o.s.}} \rho(s)ds\,,$$ (2.14)

where $\Delta\Omega$ is the region of the sky observed and $\rho(s)$ is the NFW dark-matter-halo density profile at a distance s from the Earth. Then the neutrino flux from dark-matter decay in the Milky Way Galaxy is given by

$$\frac{d\Phi(\Delta\Omega, E)}{dE} = \frac{1}{4\pi} \frac{1}{m_\psi \tau_\psi} J(\Delta\Omega)\Delta\Omega \sum_i \frac{dN_i}{dE}\,,$$ (2.15)

where m_ψ and τ_ψ are the mass and lifetime of the dark matter particles, respectively, and dN_i/dE is the energy spectrum of neutrinos of flavor i. We consider the 2π sr toward the galactic center. This gives

$$J\,(2\pi\,\text{toward the galactic center}) \simeq 2.3 \times 10^{22}\,\text{GeV/cm}^2.$$ (2.16)

The effective area of the IceCube/DeepCore detector is given by

$$A(E) \simeq \rho_{\text{ice}} N_{\text{A}} \sigma_{\nu N}^{\text{CC}}(E) V(E)\,,$$ (2.17)

where $\rho_{\text{ice}} \simeq 0.9$ g/cm^3, $N_{\text{A}} = 6.022 \times 10^{23}$ g^{-1}, $\sigma_{\nu N}^{\text{CC}}(E)$ is the charged-current neutrino-nucleon cross section [29] (for antineutrinos we must use the antineutrino-nucleon cross section, $\sigma_{\bar{\nu}N}^{\text{CC}}$) and $V(E)$ is the effective volume of the detector; for the

relevant energy range, it is a good approximation to take $V(E) \simeq 0.04 \, \mathrm{km}^3$ [30]. We have parameterized $\sigma_{\nu N}^{\mathrm{CC}}(E)$ as a fifth-degree polynomial in E to better than 6% over the range $60 \, \mathrm{GeV} \leq E \leq 10000 \, \mathrm{GeV}$,

$$\sigma_{\nu N}^{\mathrm{CC}}(E) \simeq \sum_{i=0}^{5} c_i \epsilon^i \, , \qquad (2.18)$$

where $\epsilon = E/(1\mathrm{GeV})$, $c_0 = 6.35 \times 10^{-38} \, \mathrm{cm}^2$, $c_1 = 6.82 \times 10^{-39} \, \mathrm{cm}^2$, $c_2 = -5.82 \times 10^{-43} \, \mathrm{cm}^2$, $c_3 = 1.10 \times 10^{-46} \, \mathrm{cm}^2$, $c_4 = -1.37 \times 10^{-50} \, \mathrm{cm}^2$ and $c_5 = 6.27 \times 10^{-55} \, \mathrm{cm}^2$. We have also parameterized $\sigma_{\bar{\nu} N}^{\mathrm{CC}}(E)$ as a fifth-degree polynomial in E to better than 0.5% over the range $60 \, \mathrm{GeV} \leq E \leq 10000 \, \mathrm{GeV}$,

$$\sigma_{\bar{\nu} N}^{\mathrm{CC}}(E) \simeq \sum_{i=0}^{5} \bar{c}_i \epsilon^i \, , \qquad (2.19)$$

where $\bar{c}_0 = 1.12 \times 10^{-38} \, \mathrm{cm}^2$, $\bar{c}_1 = 3.65 \times 10^{-39} \, \mathrm{cm}^2$, $\bar{c}_2 = -1.37 \times 10^{-43} \, \mathrm{cm}^2$, $\bar{c}_3 = 2.61 \times 10^{-47} \, \mathrm{cm}^2$, $\bar{c}_4 = -3.66 \times 10^{-51} \, \mathrm{cm}^2$, $\bar{c}_5 = 1.77 \times 10^{-55} \, \mathrm{cm}^2$.

The main background consists of atmospheric neutrinos. The background fluxes over a half-sky for ν_μ and $\bar{\nu}_\mu$ are given by Ref. [32]. We have fit the numerical data with the following functions (inspired by Ref. [31]):

$$\frac{d\Phi_{\nu_\mu}}{dE} = a_{\nu_\mu} \epsilon^{-b_{\nu_\mu}} \left[\frac{\log\left(1 + c_{\nu_\mu}\epsilon\right)}{c_{\nu_\mu}\epsilon} + d_{\nu_\mu} \frac{\log\left(1 + e_{\nu_\mu}\epsilon\right)}{e_{\nu_\mu}\epsilon} \right] \left(\mathrm{cm}^2 \, \mathrm{s} \, \mathrm{GeV}\right)^{-1} \, , \qquad (2.20)$$

where $\epsilon = E/(1 \, \mathrm{GeV})$, $a_{\nu_\mu} = 66.20$, $b_{\nu_\mu} = 1.96$, $c_{\nu_\mu} = 3730.61$, $d_{\nu_\mu} = -0.000011$ and $e_{\nu_\mu} = 0.014$ and

$$\frac{d\Phi_{\bar{\nu}_\mu}}{dE} = a_{\bar{\nu}_\mu} \epsilon^{-b_{\bar{\nu}_\mu}} \left[\frac{\log\left(1 + c_{\bar{\nu}_\mu}\epsilon\right)}{c_{\bar{\nu}_\mu}\epsilon} + d_{\bar{\nu}_\mu} \frac{\log\left(1 + e_{\bar{\nu}_\mu}\epsilon\right)}{e_{\bar{\nu}_\mu}\epsilon} \right] \left(\mathrm{cm}^2 \, \mathrm{s} \, \mathrm{GeV}\right)^{-1} \, , \qquad (2.21)$$

where $a_{\bar{\nu}_\mu} = 1.26$, $b_{\bar{\nu}_\mu} = 2.09$, $c_{\bar{\nu}_\mu} = 35.56$, $d_{\bar{\nu}_\mu} = -0.00051$ and $e_{\bar{\nu}_\mu} = 0.0080$. The expressions for $d\Phi_{\nu_\mu}/dE$ and $d\Phi_{\bar{\nu}_\mu}/dE$ are good to better than 6% and 8%,

11

respectively, over the range $60\,\text{GeV} \le E \le 10000\,\text{GeV}$.

The rate of neutrino events between energies $E_{\min}$ and $E_{\max}$ is given by

$$\Gamma = \int_{E_{\min}}^{E_{\max}} dE\, A(E) \frac{d\Phi(\Delta\Omega)}{dE}. \tag{2.22}$$

2.3 Gamma-Ray Propagation

The gamma-ray flux from dark-matter decay consists of multiple components.

First of all, we have a gamma-ray flux which is due to photons created in the decay shower. We will call this the *local* contribution to the gamma-ray flux. The component of this flux which is due to dark-matter decays in the Milky Way Galaxy can be computed using Eq. (2.15) where the sum over dN_i/dE is now the energy spectrum of photons created in the dark-matter decay. There is also an isotropic extragalactic component. Gamma rays originating at cosmological distances experience a significant red shift as they travel to the Milky Way Galaxy due to the expansion of the universe. The extragalactic flux measured at the Earth at a particular energy E is due to gamma rays originally produced at higher energies in distant galaxies; as these gamma rays traveled to the Earth, their energies were red-shifted down to E. The more distant the galaxy in which they originated, the greater the red shift experienced by the gamma rays. The explicit expression for the extragalactic flux, which is essentially an integral over all red shifts, is given by (see, e.g., Refs. [33] and [34])

$$\left(\frac{d\Phi_\gamma}{dE\,d\Omega}\right)_{\text{local}}^{\text{(ex.)}} = \frac{c}{4\pi} \frac{\Omega_{\text{DM}}\rho_c}{m_\psi \tau_\psi} \int_0^\infty dz \frac{1}{H(z)} \frac{dN_\gamma}{d\,(E(1+z))}, \tag{2.23}$$

where $\Omega_{\text{DM}} \simeq 0.21$, $\rho_c \simeq 5.46 \times 10^{-6}\,\text{GeV/cm}^3$, z is the redshift and

$$H(z) = H_0 \sqrt{\Omega_{\text{M}}(1+z)^3 + (1 - \Omega_{\text{M}})}, \tag{2.24}$$

where $H_0 \simeq 72 \ (\text{km/s}) \, /\text{Mpc}$ and $\Omega_\text{M} \simeq 0.26$.

There is also a flux due to synchotron radiation produced by electrons and positrons interacting with the galactic magnetic field. Since the field is so weak, this contribution is negligible at gamma-ray frequencies [33].

The second major component of the gamma-ray flux is due to inverse Compton scattering of electrons and positrons produced in the dark-matter decay chain off of interstellar/intergalactic photons. The interstellar radiation field (ISRF) consists of three main components (see, e.g., Ref. [40]): cosmic microwave background (CMB) radiation, starlight and infrared radiation from interstellar dust. The CMB component is constant throughout the galaxy, and the number density is given by the blackbody spectrum

$$n_\text{CMB}(E) = \frac{E^2}{\pi^2} \frac{1}{e^{E/T_0} - 1} \, , \tag{2.25}$$

where $T_0 \simeq 2.725 \,\text{K}$. The other components are given by the GALPROP collaboration [41]. Since we will be comparing our predictions to the Fermi LAT measurements of the *extragalactic* diffuse gamma-ray emission [39], we need not concern ourselves with the *interstellar* radiation field. On cosmological scales, the only significant component of the radiation field is due to the cosmic microwave background. To compute the gamma-ray flux from inverse Compton scattering on cosmological scales, we will follow the prescription given in Ref. [42].

Since typical CMB photon energies are relatively small, we can work in the Thomson (non-relativistic) limit for which the radiated power is given by

$$\mathcal{P}_\text{IC} \left(E_\gamma, E_e, z \right) = \frac{3\sigma_\text{T}}{4\gamma^2} E_\gamma \int_0^1 dy \, \frac{n_\text{CMB} \left(E_\gamma^0(y), z \right)}{y} \left(2y \log y + y + 1 - 2y^2 \right) , \tag{2.26}$$

where $\sigma_\text{T} \simeq 6.65 \times 10^{-25} \,\text{cm}^2$ is the Thomson cross section,

$$y = \frac{E_\gamma}{4\gamma^2 E_\gamma^0} \tag{2.27}$$

13

and

$$\gamma = \frac{E_e}{m_e}.$$

(2.28)

From Ref. [33], the rate of energy loss due to inverse Compton scattering in the Thomson limit is given by

$$b_{\mathrm{IC}} = \frac{4}{3} \left(\frac{E}{m_e} \right)^2 \sigma_{\mathrm{T}} \rho_{\mathrm{CMB}} \left(1 + z \right)^4 ,$$

(2.29)

where $\rho_{\mathrm{CMB}} \simeq 0.26 \,\mathrm{eV/cm^3}$. Then the emissivity of gamma-rays from inverse Compton scattering is given by

$$j_{\mathrm{IC}} \left(E', z' \right) = \int_{m_e}^{m_\psi/2} dE_e \frac{\mathcal{P}_{\mathrm{IC}} \left(E'_\gamma, E_e, z' \right)}{b_{\mathrm{IC}} \left(E_e, z' \right)} \int d\bar{E}_e \frac{dN_e}{d\bar{E}} \frac{\bar{\rho}(z')}{m_\psi \tau_\psi} ,$$

(2.30)

where $\bar{\rho}(z) = \bar{\rho}_0 (1 + z)^3$ with $\bar{\rho}_0 \simeq 1.15 \times 10^{-6} \,\mathrm{GeV/cm^3}$ and dN_e/dE is the energy spectrum of electrons and positrons produced in the dark-matter decay. In the Thomson limit, we can simplify the expression for the emissivity to

$$j_{\mathrm{IC}} \left(E', z' \right) = \left(1 + z \right)^2 j_{\mathrm{IC}} \left(\frac{E'}{1 + z'}, 0 \right).$$

(2.31)

Then the gamma-ray flux from extragalactic inverse Compton scattering is given by

$$\left(\frac{d\Phi_{\mathrm{IC}}}{dE_\gamma d\Omega} \right)_{\mathrm{IC}}^{(\mathrm{ex.})} = \frac{c}{E_\gamma} \int_0^\infty dz' \frac{1}{H(z')(1 + z')^4} \frac{j_{\mathrm{IC}} \left(E'_\gamma, z' \right)}{4\pi} e^{-\tau(E'_\gamma, z')} ,$$

(2.32)

where $E'_\gamma = E_\gamma(1 + z')$, $H(z')$ is given by Eq. (2.24) and $\tau(E'_\gamma, z')$ is the optical depth of the universe for gamma rays collected today with energy $E_\gamma = E'_\gamma/(1 + z')$. Several processes contribute to the value of the optical depth. In the energy range $1 \,\mathrm{Mev} \lesssim E \lesssim 1 \,\mathrm{TeV}$, the factor $e^{-\tau(E'_\gamma, z')}$ accounts for the absorption of gamma rays by pair production on baryonic matter, photon-photon scattering on ambient photon background radiation (PBR) and pair production on ambient PBR [42]. From

14

Ref. [43], we see that $e^{-\tau}$ is close to 1 in the region of interest, so we will assume $e^{-\tau} = 1$ from this point on.

Chapter 3

Three-Body Decays

In the propagation models described in Ch. 2, the only remaining undetermined quantities are m_ψ, τ_ψ and dN_k/dE where k is meant to represent electrons, positrons, neutrinos, antineutrinos or photons. The energy spectra, dN_k/dE are determined by m_ψ and by a set of parameters which I describe in the following section. We consider decays of the form

$$\psi \to \ell_i^+ \ell_j^- \nu \,, \tag{3.1}$$

where $\ell_i^\pm$ is a charged lepton of the ith generation. At this point, the ν need not be a neutrino; it can be any neutral fermion which is much lighter than ψ. The exact nature of this light neutral state will be irrelevant for the $e^\pm$ and gamma-ray analyses since its effect on the results presented in those sections will come solely from kinematics. For the sake of convenience, however, we will refer to ν as a neutrino. We focus on the simplest scenario, in which there are no additional decay channels involving the charge conjugate of ν, and consider the possible four-fermion operators that contribute to the decays of interest. Note that the production of a neutrino in the primary decay may have interesting phenomenological consequences (see, e.g., Ref. [17]), which provides a separate motivation for our three-fermion final state.

3.1 Four-Fermion Operators

The problem of paramterizing an unknown decay amplitude of one spin-1/2 particle to three distinct spin-1/2 decay products was encountered in the study of muon decay, before the Standard Model was well-established. The most general decay amplitude $\mathcal{M}$ can be parameterized by [20]

$$i\mathcal{M} = ig \sum_i \left[\bar{u}(p_0)O_i u_\psi\right] \left[\bar{u}(p_-)O_i(c_i + c_i'\gamma^5)v(p_+)\right] , \tag{3.2}$$

where $p_\pm$ and p_0 are the momenta of the decay products, labeled according to their electric charge, and the O_i, $i = 1 \cdots 5$ are elements of the set of linearly independent matrices

$$O = \{1, \gamma^\mu, \sigma^{\mu\nu}, \gamma^\mu\gamma^5, \gamma^5\} . \tag{3.3}$$

The c_i and c_i' are complex coefficients. Terms involving the contraction of spinor indices that link different pairs of spinor wave functions can be recast in the form of Eq. (3.2) via Fierz transformations. Since the final state particles are much lighter than the dark matter candidate (which is at the TeV scale), we can safely neglect their masses.

Since the neutral final state particle is stable, the energy spectra of electrons and positrons that are observed at cosmic-ray observatories are determined by the energy spectra of the the charged leptons, ℓ^+ and ℓ^-, that are produced in the primary decay; this follows from the differential decay distribution

$$\frac{1}{\Gamma}\frac{d^2\Gamma}{dE_0 dE_\pm} = \frac{1}{64\pi^3 m_\psi}\langle|\mathcal{M}|^2\rangle , \tag{3.4}$$

where $\langle|\mathcal{M}|^2\rangle$ is the spin-summed/averaged squared amplitude. This quantity can be evaluated exactly from Eq. (3.2) using FeynCalc [21], and the $\ell^\pm$ energy distribution can be computed by integrating over the neutral lepton energy E_0. The result contains

terms quadratic and cubic in $E_\pm$; however, since the distribution must be normalized to unity, the result has the following simple parametrization:

$$\frac{1}{\Gamma}\frac{d\Gamma}{dE_\pm} = \frac{1}{m_\psi}\frac{E_\pm^2}{m_\psi^2}\left[\xi_\pm + \left(64 - \frac{8}{3}\xi_\pm\right)\frac{E_\pm}{m_\psi}\right].$$ (3.5)

Similarly, the neutrino energy distribution is given by

$$\frac{1}{\Gamma}\frac{d\Gamma}{dE_0} = \frac{1}{m_\psi}\frac{E_0^2}{m_\psi^2}\left[\xi_0 + \left(64 - \frac{8}{3}\xi_0\right)\frac{E_0}{m_\psi}\right].$$ (3.6)

The requirement that these expressions remain positive over the kinematically accessible range $0 \leq E_i \leq m_\psi/2$ restricts the parameters ξ_+, ξ_- and ξ_0 to fall within the range

$$0 \leq \xi_i \leq 96.$$ (3.7)

The parameters $\xi_\pm$ and ξ_0 may be expressed in terms of the operator coefficients c_i and c_i' defined in Eq. (3.2):

$$\xi_j = 48\,\frac{\mathbf{c}^\dagger N_j\,\mathbf{c} + \mathbf{c}'^\dagger N_j\,\mathbf{c}'}{\mathbf{c}^\dagger D\,\mathbf{c} + \mathbf{c}'^\dagger D\,\mathbf{c}'},$$ (3.8)

where $j = \pm, 0$, $\mathbf{c} = [c_1, c_2, c_3, c_4, c_5]^T$ and $\mathbf{c}' = [c_1', c_2', c_3', c_4', c_5']^T$. The five-by-five matrices N_j and D are given by

$$N_\pm = \begin{pmatrix} 1 & 0 & \mp 2 & 0 & 0 \\ 0 & 6 & 0 & \pm 2 & 0 \\ \mp 2 & 0 & 40 & 0 & \mp 2 \\ 0 & \pm 2 & 0 & 6 & 0 \\ 0 & 0 & \mp 2 & 0 & 1 \end{pmatrix},$$ (3.9)

18

$$
N_0 = \begin{pmatrix} 2 & 0 & 0 & 0 & 0 \\ 0 & 4 & 0 & 0 & 0 \\ 0 & 0 & 16 & 0 & 0 \\ 0 & 0 & 0 & 4 & 0 \\ 0 & 0 & 0 & 0 & 2 \end{pmatrix}
$$

(3.10)

and

$$
D = \begin{pmatrix} 1 & 0 & 0 & 0 & 0 \\ 0 & 4 & 0 & 0 & 0 \\ 0 & 0 & 24 & 0 & 0 \\ 0 & 0 & 0 & 4 & 0 \\ 0 & 0 & 0 & 0 & 1 \end{pmatrix}.
$$

(3.11)

3.2   Single Differential Decay Distributions

Since we have a relatively simple expression, Eq. (3.5), for the most general decay distributions for the charged leptons in the decay $\psi \to \ell_i^+ \ell_j^- \nu$, it would be preferable to work in terms of these *single*-differential decay distributions as opposed to the double-differential decay distributions given by Eq. (3.4). In this section we will prove that the energy spectra of electrons, positrons, neutrinos, antineutrinos and photons created in the decay shower can be expressed solely in terms of single-differential decay distributions. From a phenomenological point of view, then, there is no need to bother with the double differential of Eq. (3.4); the decay is entirely characterized by the single differentials

$$
\frac{1}{\Gamma} \frac{d\Gamma}{dE_k} ,
$$

(3.12)

where k runs over the three decay products.

The decay is completely characterized by the double-differential decay distribution

$$\frac{1}{\Gamma}\frac{\partial^2\Gamma}{\partial E_{\ell_i^+}\partial E_\nu}\,,\tag{3.13}$$

where $E_{\ell_i^+}$ is the energy of the ℓ_i^+ particle in the initial three-body decay – not the energy of any ℓ_i^+ particles created in the ensuing shower – and E_ν is the energy of the neutrino in the initial three-body decay – not the energy of any neutrinos created in the ensuing shower. For any $E_{\ell_i^+}$ and E_ν, let

$$\frac{dn\left(E_{\ell_i^+}, E_\nu\right)}{dE_{e^+}}\tag{3.14}$$

be the energy spectrum of positrons for that particular set of ℓ_i^+, ℓ_j^- and ν energies. Note that $E_{\ell_j^-} = M_\psi - \left(E_{\ell_i^+} + E_\nu\right)$, so it is only necessary to specify two of the three energies. There is implicit E_{e^+} dependence in Eq. (3.14). The total positron energy spectrum is then given by

$$\frac{dN}{dE_{e^+}} = \iint dE_{\ell_i^+}dE_\nu \frac{1}{\Gamma}\frac{\partial^2\Gamma}{\partial E_{\ell_i^+}\partial E_\nu}\frac{dn\left(E_{\ell_i^+}, E_\nu\right)}{dE_{e^+}}\,,\tag{3.15}$$

where the integrations run over all kinematically allowed values of $E_{\ell_i^+}$ and E_ν.

The double differential given in Eq. (3.13) above is a function of $E_{\ell_i^+}$ and E_ν. This is a vestige of the tendency to integrate out the $E_{\ell_j^-}$ dependence first when evaluating Γ. But we could just as well characterize the decay by the double differential

$$\frac{1}{\Gamma}\frac{\partial^2\Gamma}{\partial E_{\ell_i^+}\partial E_{\ell_j^-}}.\tag{3.16}$$

Then, for any $E_{\ell_i^+}$ and $E_{\ell_j^-}$, we can define

$$\frac{d\tilde{n}\left(E_{\ell_i^+}, E_{\ell_j^-}\right)}{dE_{e+}} \tag{3.17}$$

to be the positron energy spectrum for that particular set of ℓ_i^+, ℓ_j^- and ν energies. And so, echoing Eq. (3.15), the total positron energy spectrum is given by

$$\frac{dN}{dE_{e+}} = \iint dE_{\ell_i^+} dE_{\ell_j^-} \frac{1}{\Gamma} \frac{\partial^2 \Gamma}{\partial E_{\ell_i^+} \partial E_{\ell_j^-}} \frac{d\tilde{n}\left(E_{\ell_i^+}, E_{\ell_j^-}\right)}{dE_{e+}}, \tag{3.18}$$

where the integrations run, as above, over all kinematically allowed values of $E_{\ell_i^+}$ and $E_{\ell_j^-}$.

Now,

$$\frac{d\tilde{n}\left(E_{\ell_i^+}, E_{\ell_j^-}\right)}{dE_{e+}} \tag{3.19}$$

is the energy spectrum of positrons created in the decays of an ℓ_i^+ with energy $E_{\ell_i^+}$, an ℓ_j^- with energy $E_{\ell_j^-}$ and a ν with energy $E_\nu = M_\psi - \left(E_{\ell_i^+} + E_{\ell_j^-}\right)$. This is the same as the *sum* of the energy spectra of the ℓ_i^+ decay, the ℓ_j^- decay and the ν decay. That is, once we have fixed the energies of the ℓ_i^+, the ℓ_j^- and the ν, we can consider their decays independently. We then have

$$\frac{d\tilde{n}\left(E_{\ell_i^+}, E_{\ell_j^-}\right)}{dE_{e+}} = \frac{d\tilde{n}_{\ell_i^+}\left(E_{\ell_i^+}\right)}{dE_{e+}} + \frac{d\tilde{n}_{\ell_j^-}\left(E_{\ell_j^-}\right)}{dE_{e+}} + \frac{d\tilde{n}_\nu\left(E_\nu\right)}{dE_{e+}}, \tag{3.20}$$

where the terms with only one argument are the positron energy spectra for the decays of each individual particle at a particular energy. Note that

$$\frac{d\tilde{n}_\nu\left(E_\nu\right)}{dE_{e+}} = 0, \tag{3.21}$$

so

$$\frac{d\tilde{n}\left(E_{\ell_i^+}, E_{\ell_j^-}\right)}{dE_{e+}} = \frac{d\tilde{n}_{\ell_i^+}\left(E_{\ell_i^+}\right)}{dE_{e+}} + \frac{d\tilde{n}_{\ell_j^-}\left(E_{\ell_j^-}\right)}{dE_{e+}}. \tag{3.22}$$

Now we substitute Eq. (3.22) into the double integral [Eq. (3.18)] to obtain

$$\frac{dN}{dE_{e+}} = \iint dE_{\ell_i^+} dE_{\ell_j^-} \frac{1}{\Gamma}\frac{\partial^2\Gamma}{\partial E_{\ell_i^+}\partial E_{\ell_j^-}}\left[\frac{d\tilde{n}_{\ell_i^+}\left(E_{\ell_i^+}\right)}{dE_{e+}} + \frac{d\tilde{n}_{\ell_j^-}\left(E_{\ell_j^-}\right)}{dE_{e+}}\right], \tag{3.23}$$

where, as above, the integral runs over all kinematically allowed values of $E_{\ell_i^+}$ and $E_{\ell_j^-}$. Then we can break the integral into two parts and choose a different order of integration for each term. This gives

$$\begin{aligned}\frac{dN}{dE_{e+}} &= \int_0^{M_\psi/2}\int_{M_\psi/2-E_{\ell_i^+}}^{M_\psi/2} dE_{\ell_j^-} dE_{\ell_i^+} \frac{1}{\Gamma}\frac{\partial^2\Gamma}{\partial E_{\ell_i^+}\partial E_{\ell_j^-}}\frac{d\tilde{n}_{\ell_i^+}\left(E_{\ell_i^+}\right)}{dE_{e+}} \\ &+ \int_0^{M_\psi/2}\int_{M_\psi/2-E_{\ell_i^-}}^{M_\psi/2} dE_{\ell_i^+} dE_{\ell_j^-} \frac{1}{\Gamma}\frac{\partial^2\Gamma}{\partial E_{\ell_i^+}\partial E_{\ell_j^-}}\frac{d\tilde{n}_{\ell_j^-}\left(E_{\ell_j^-}\right)}{dE_{e+}}.\end{aligned} \tag{3.24}$$

Note that, in the integrand of the first term, the dependence on $E_{\ell_j^-}$ comes entirely from the double-differential decay distribution. Similarly, in the integrand of the second term, the dependence on $E_{\ell_i^+}$ comes entirely from the double-differential decay distribution. This was the motivation for the different orders of integration. It is now easy to see that the inner integrations (over $E_{\ell_j^-}$ in the first term on the right and over $E_{\ell_i^+}$ in the second term) simply turn the double-differential decay distributions into single-differential decay distributions; this gives

$$\frac{dN}{dE_{e+}} = \int_0^{M_\psi/2} dE_{\ell_i^+} \frac{1}{\Gamma}\frac{d\Gamma}{dE_{\ell_i^+}}\frac{d\tilde{n}_{\ell_i^+}\left(E_{\ell_i^+}\right)}{dE_{e+}} + \int_0^{M_\psi/2} dE_{\ell_j^-} \frac{1}{\Gamma}\frac{d\Gamma}{dE_{\ell_j^-}}\frac{d\tilde{n}_{\ell_j^-}\left(E_{\ell_j^-}\right)}{dE_{e+}}. \tag{3.25}$$

The first term on the right is the positron energy spectrum due to the decays of ℓ_i^+

22

particles with an energy distribution given by

$$\frac{1}{\Gamma}\frac{d\Gamma}{dE_{\ell_i^+}},\tag{3.26}$$

and the second term on the right is the positron energy spectrum due to the decays ℓ_j^- particles with an energy distribution given by

$$\frac{1}{\Gamma}\frac{d\Gamma}{dE_{\ell_j^-}}.\tag{3.27}$$

Therefore, given expressions for Eq. (3.26) and Eq. (3.27), we can compute dN/dE_{e^+} without any reference to the underlying double differential, Eq. (3.4).

The analysis is obviously identical for the electron energy spectrum. For photons, it will also be the same, since the ν is stable and, hence, Eqs. (3.21) and (3.25) still holds with $e^+ \rightarrow \gamma$. If we assume that ν is a neutrino (as opposed to an antineutrino), then the antineutrino energy spectrum, $dN/dE_{\bar{\nu}}$, will similarly be given by Eq. (3.25) with $e^+ \rightarrow \bar{\nu}$. For neutrinos, the analog of Eq. (3.21) is

$$\frac{d\tilde{n}_\nu\left(E'_\nu\right)}{dE_\nu} = \delta\left(E_\nu - E'_\nu\right).\tag{3.28}$$

Then, by a similar analysis, the analog of Eq. (3.25) is

$$\frac{dN}{dE_\nu} = \int_0^{M_\psi/2} dE_{\ell_i^+}\frac{1}{\Gamma}\frac{d\Gamma}{dE_{\ell_i^+}}\frac{d\tilde{n}_{\ell_i^+}\left(E_{\ell_i^+}\right)}{dE_\nu} + \int_0^{M_\psi/2} dE_{\ell_j^-}\frac{1}{\Gamma}\frac{d\Gamma}{dE_{\ell_j^-}}\frac{d\tilde{n}_{\ell_j^-}\left(E_{\ell_j^-}\right)}{dE_\nu} + \frac{1}{\Gamma}\frac{d\Gamma}{dE_\nu}.\tag{3.29}$$

Once again, we see that the single differentials completely characterize the energy spectrum. The only difference is that we must now pay attention to the single-differential decay distribution of the ν.

Chapter 4

Results

We consider dark-matter decays of the form $\psi \to \ell_i^+ \ell_j^- \nu$ where $\ell_i^\pm$ is a charged lepton of the ith generation and ν is a neutrino. We will not specify a neutrino flavor, since, as we will see below, it is of little significance. For each decay, we used PYTHIA [22] to simulate the shower of decays down to stable particles. It is then a simple matter to extract the energy spectra of electrons, positrons, neutrinos, antineutrinos and photons created in the process as a whole.

There are nine (3×3) possible decay channels, and we require

$$\sum_{i,j} B(\ell_i^+ \ell_j^- \nu) = 1 \,, \tag{4.1}$$

where $B(\ell_i^+ \ell_j^- \nu)$ is the branching fraction for $\psi \to \ell_i^+ \ell_j^- \nu$. Then we have

$$\frac{dN_{e^\pm}}{dE} = \sum_{i,j} B(\ell_i^+ \ell_j^- \nu) \left(\frac{dN_{e^\pm}}{dE} \right)_{ij} \,, \tag{4.2}$$

where $(dN_{e^\pm}/dE)_{ij}$ is the electron/positron energy spectrum for $\psi \to \ell_i^+ \ell_j^- \nu$. The energy spectra of neutrinos, antineutrinos and photons are given by similar expressions.

In Sec. 3.1, we showed that the energy spectra of the leptons in the decay $\psi \to \ell_i^+ \ell_j^- \nu$ are characterized by the ordered triplet (ξ_+, ξ_-, ξ_0), where $0 \leq \xi_i \leq 96$. In

Sec. 3.2, we showed that $(dN_{e^\pm}/dE)_{ij}$, $(dN_{\bar{\nu}}/dE)_{ij}$, and $(dN_\gamma/dE)_{ij}$ are entirely determined by m_ψ and the ordered *pair* (ξ_+, ξ_-). For $(dN_\nu/dE)_{ij}$, we also need to know ξ_0. For decays involving more than one channel (e.g., $\psi \to e^+\mu^-\nu$ and $\psi \to \mu^+\tau^-\nu$), we assume a constant (ξ_+, ξ_-, ξ_0). Then, since the branching fractions are subject to Eq. (4.1), we can determine all of the dN/dE by specifying m_ψ, ξ_+, ξ_-, ξ_0 and eight of the nine branching fractions.

To summarize, when we use the cosmic-ray propagation models described in Ch. 2, the resulting electron, positron, neutrino, antineutrino and photon fluxes measured at the top of the Earth's atmosphere are determined by 12 parameters: m_ψ, ξ_+, ξ_-, ξ_0 and eight of the nine branching fractions.

4.1   Electron-Positron Flux

For the $e^\pm$ fluxes, ξ_0 is irrelevant, since ν is stable. So rather than talking about the triplet (ξ_+, ξ_-, ξ_0), we need only concern ourselves with the *pair* (ξ_+, ξ_-).

For each of the decay scenarios considered below, we fixed (ξ_+, ξ_-) and the branching fractions and then performed a χ^2 fit to the PAMELA, Fermi LAT, H.E.S.S. 2008 and H.E.S.S. 2009 data with m_ψ and τ_ψ as fitting parameters. We allowed m_ψ to vary in increments of $500\,\mathrm{GeV}$, and we allowed τ_ψ to vary in increments of $0.1 \times 10^{26}\,\mathrm{s}$. We consider the range $E > 10\,\mathrm{GeV}$, where the effects of a TeV-scale dark-matter candidate are relevant. Where the high-energy and low-energy Fermi LAT data overlap, we have plotted only the high-energy data. We omit from our figures the H.E.S.S. bands of systematic uncertainty.

Leaving m_ψ and τ_ψ as free variables, we find that the results are relatively insensitive to the choice of (ξ_+, ξ_-). This is demonstrated for the pure decay $\psi \to \tau^+\tau^-\nu$ in Fig. 4.1 where the envelope of possible cosmic-ray spectra is shown; that is, when the (ξ_+, ξ_-) parameter space is sampled, all of the resulting curves fall between those
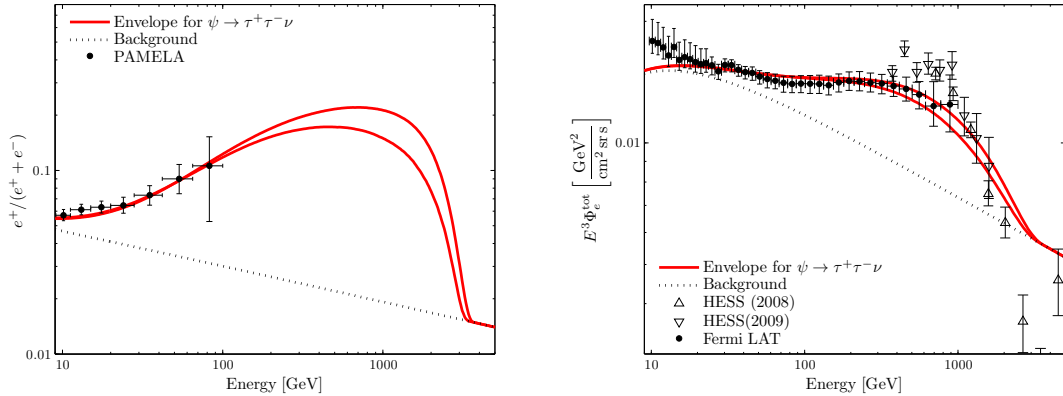
Figure 4.1: The envelope of possible cosmic-ray spectra for $\psi \to \tau^+\tau^-\nu$. Ranges of the fit parameters are given in the text.

plotted in Fig. 4.1. For the example shown, m_ψ varies between 6.5 and 8.5 TeV while τ_ψ varies between 0.5×10^{26} s and 0.7×10^{26} s; the χ^2 per degree of freedom (χ^2/d.o.f.) remains between 0.5 and 0.6. We performed the same analysis on the other decay scenarios discussed below and found a similar behavior. As such, we take $(\xi_+, \xi_-) = (48, 48)$ for the remaining results that we present.

As a starting point, we show the cosmic-ray spectra for some charged-lepton-flavor-conserving decays in Fig. 4.2. We consider the pure decays $\psi \to \mu^+\mu^-\nu$ and $\psi \to \tau^+\tau^-\nu$, and we also consider the flavor-democratic decay for which $B(\ell_i^+\ell_i^-\nu) = 1/3$ for all i. For $\psi \to \mu^+\mu^-\nu$, we have a χ^2/d.o.f. of approximately 0.9. For $\psi \to \tau^+\tau^-\nu$, we have χ^2/d.o.f. $\approx$ 0.6. And for the flavor-democratic $\psi \to \ell^+\ell^-\nu$, we have χ^2/d.o.f. $\approx$ 0.8. These are to be contrasted with the flavor-violating decays of Fig. 4.3.

We consider three classes of flavor-violating decays:

$$\psi \to e^\pm\mu^\mp\nu, \qquad \psi \to e^\pm\tau^\mp\nu \qquad \text{and} \qquad \psi \to \mu^\pm\tau^\mp\nu. \qquad (4.3)$$

Each class contains two decay channels (e.g., $\psi \to e^+\mu^-\nu$ and $\psi \to e^-\mu^+\nu$). We
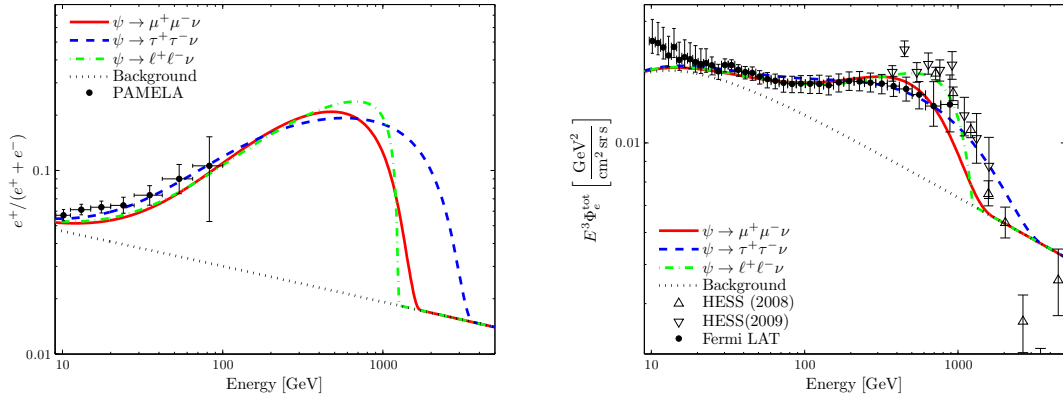
Figure 4.2: Positron fraction and total electron-positron flux for some charged-lepton-flavor-conserving decays. Best fits are shown, corresponding to the following masses and lifetimes: for $\psi \to \mu^+\mu^-\nu$, $m_\psi = 3.5$ TeV and $\tau_\psi = 1.5 \times 10^{26}$ s; for $\psi \to \tau^+\tau^-\nu$, $m_\psi = 7.5$ TeV and $\tau_\psi = 0.6 \times 10^{26}$ s; for the flavor-democratic decay $\psi \to \ell^+\ell^-\nu$, $m_\psi = 2.5$ TeV and $\tau_\psi = 1.9 \times 10^{26}$ s.

consider all six of the pure decays, i.e., decays involving only one channel. We also consider mixtures of decay channels belonging to the same class; some representative choices are shown in Fig. 4.3. Note that, for fixed m_ψ and τ_ψ, the total electron-positron flux – which does not distinguish between the two electric charges – is the same for any two decays belonging to the same class. For this reason, we require only one plot of the total flux in Fig. 4.3. We find that the χ^2 is relatively flat as a function of the branching fraction within each class of decays: over the range of possible branching fractions, we find that the χ^2/d.o.f. varies by no more than 10% from 1.2, 1.1 and 0.6, for $\psi \to e^\pm\mu^\mp\nu$, $\psi \to e^\pm\tau^\mp\nu$, and $\psi \to \mu^\pm\tau^\mp\nu$, respectively. Different choices than the ones shown for the branching fraction within a given class describe the existing data well but provide different predicted spectra that interpolate between the curves shown. Note that the distinctive dip in the $\mu^+e^-\nu$ and $\tau^+e^-\nu$ positron fractions around 1 TeV is due to the hard electron produced in the initial decay; this greatly enhances the electron to positron ratio in the high energy bins, leading to a suppression in the positron fraction for fixed total flux.
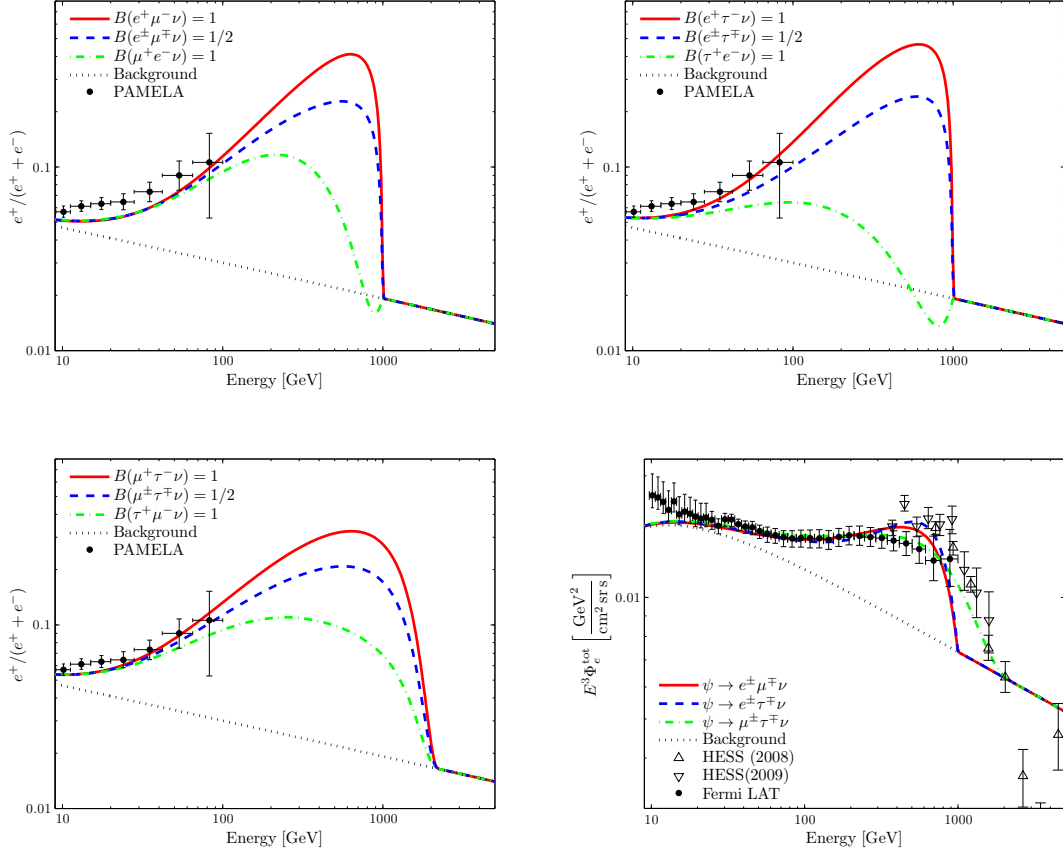
Figure 4.3: Positron fraction and total electron-positron flux for some charged-lepton-flavor-violating decays with various sets of branching fractions. Best fits are shown, corresponding to the following masses and lifetimes: for $\psi \to e^{\pm}\mu^{\mp}\nu$, $m_{\psi} = 2.0$ TeV and $\tau_{\psi} = 2.9 \times 10^{26}$ s; for $\psi \to e^{\pm}\tau^{\mp}\nu$, $m_{\psi} = 2.0$ TeV and $\tau_{\psi} = 2.4 \times 10^{26}$ s; for $\psi \to \mu^{\pm}\tau^{\mp}\nu$, $m_{\psi} = 4.5$ TeV and $\tau_{\psi} = 1.0 \times 10^{26}$ s.

The results presented in this section show that a variety of possible lepton-flavor-violating decay modes for a spin-1/2, charge-asymmetric dark-matter candidate can describe existing data well, as quantified by the χ^2 per degree of freedom for the best fits to the data. Significantly, the results for the predicted positron fraction differ substantially for energies above $\sim 100\,\mathrm{GeV}$, the maximum for which the PAMELA experiment is sensitive. In some cases, more precise measurement of the total electron-positron flux around 1 TeV may also provide a means of distinguishing these scenarios. Future data from experiments like AMS-02 [18], which can probe these energy ranges of the predicted spectra, may determine whether the possibilities discussed in this section present viable descriptions of the cosmic-ray spectrum.

4.2   Gamma-Ray Flux

We compute the extragalactic gamma-ray flux due to dark-matter decays by using the prescription given in Sec. 2.3. This is to be compared to the Fermi LAT extragalactic gamma-ray background (EGB) data [39]. Contributions to this background may include active galactic nuclei, starburst galaxies and gamma-ray bursts. Since there is no widely accepted model for the extragalactic gamma-ray background, our goal in this section is not to fit the data but simply to place an upper bound on the gamma-ray flux from dark-matter decay.

In Fig. 4.4, we have plotted the gamma-ray fluxes for several decays discussed in Sec. 4.1 together with the Fermi LAT extragalactic gamma-ray background data. In each case, we have used the best-fit values for m_ψ and τ_ψ. Note that the photon flux from $\psi \to \ell_i^+ \ell_j^- \nu$ is the same as the photon flux from $\psi \to \ell_j^+ \ell_i^- \nu$. We have also separated the gamma-ray flux from dark matter into its two components: prompt (i.e., local) gamma-rays and gamma-rays from inverse Compton scattering. We see that inverse Compton scattering dominates at lower energies while the prompt gamma-
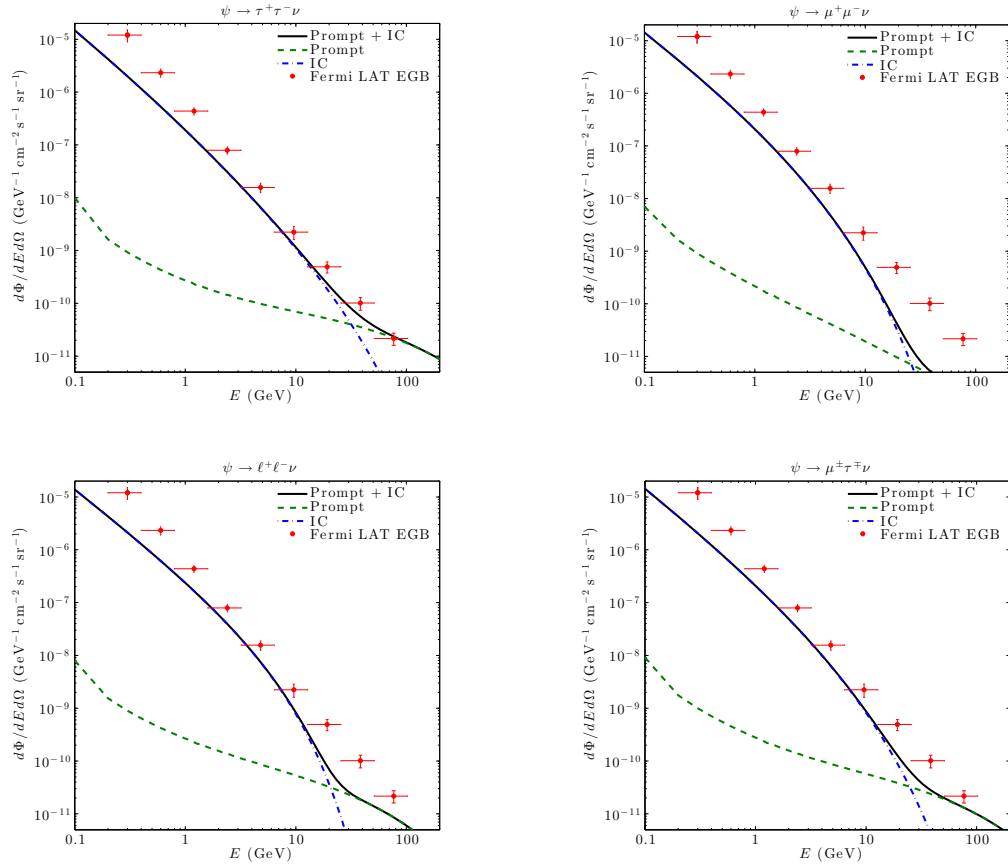
Figure 4.4: Gamma-ray flux for some flavor-conserving and flavor-violating decays. The values for m_ψ and τ_ψ are the same as those given in Figs. 4.2 and 4.3.

rays dominate at higher energies. Crucially, we see no contradiction with the Fermi LAT data; the fluxes from dark matter are nowhere in excess of the fluxes observed by the Fermi collaboration.

Of course, it is possible that dark-matter decays occur but are not solely responsible for the $e^\pm$ excesses observed by PAMELA and Fermi LAT. In this case, we can use the Fermi LAT gamma-ray data to exclude regions of the parameter space. In Sec. 4.3, we show exclusion plots for a representative sample of decays. These plots show the regions of the parameter space spanned by m_ψ and τ_ψ that are in conflict with the Fermi gamma-ray data at a statistical significance of 3σ or more.

4.3   Neutrino Flux

Following Ref. [35], we compute the predicted number of neutrino events from galactic dark-matter decay seen at IceCube/DeepCore after 5 years of running. For a given dark-matter mass, we find the lifetime below which IceCube/DeepCore would provide a 2σ exclusion or a 5σ discovery. We consider the $\nu_\mu + \bar{\nu}_\mu$ flux. Since the neutrinos from dark-matter decay will have traveled a variety of large distances, we assume that the ratio of flavors if $1:1:1$ upon arrival at the Earth due to neutrino oscillations. For this reason, the flavor of the ν in the initial three-body final state is of no significance; there is equal probability that this ν will oscillate into any of the three flavors as it travels to the Earth. The same is true of all the neutrinos created in the decay showers of the charged leptons ℓ_i^+ and ℓ_j^-. We can, therefore, take

$$\frac{dN_{\nu_\mu}}{dE} = \frac{1}{3} \sum_i \frac{dN_{\nu_i}}{dE} \qquad (4.4)$$

and

$$\frac{dN_{\bar{\nu}_\mu}}{dE} = \frac{1}{3} \sum_i \frac{dN_{\bar{\nu}_i}}{dE}. \qquad (4.5)$$

m_ψ (GeV)	$E_{\text{min.}}$ (GeV)	$E_{\text{max.}}$ (GeV)
1000	150	800
2000	300	1500
10000	1500	8000

Table 4.1: Energy bins for the neutrino flux.

IceCube/DeepCore has a limited energy resolution. In keeping with Ref. [35], we use the energies bins shown in Table 4.1.

Some results for charged-lepton-flavor-conserving decays are shown in Fig. 4.5; some results for charged-lepton-flavor-violating decays are shown in Fig. 4.6. We have actually combined the neutrino exclusion plots with the gamma-ray exclusion plots. Additionally, we have plotted the points which provide good fits to the PAMELA and Fermi LAT $e^\pm$ data as discussed in Sec. 4.1.

The "kinks" that appear at $M_\psi = 2000\,\text{GeV}$ come as a result of following the analysis of Ref. [35] in which no masses between $1000\,\text{GeV}$ and $2000\,\text{GeV}$ nor between $2000\,\text{GeV}$ and $10000\,\text{GeV}$ are considered. In order to compare our results to those of Ref. [35], we only calculate the bounds for the masses given in Table. 4.1. We have connected these points in Figs. 4.5 and 4.6 so as to give some indication of the shape of the exclusion line over the range $1000\,\text{GeV} \leq M_\psi \leq 10000\,\text{GeV}$. Note, however, that the exclusion line is not uniquely defined since there is a dependence on the energy bins ($E_{\text{min.}}$ and $E_{\text{max.}}$ as in Table. 4.1); we use the energy bins given in Ref. [35].
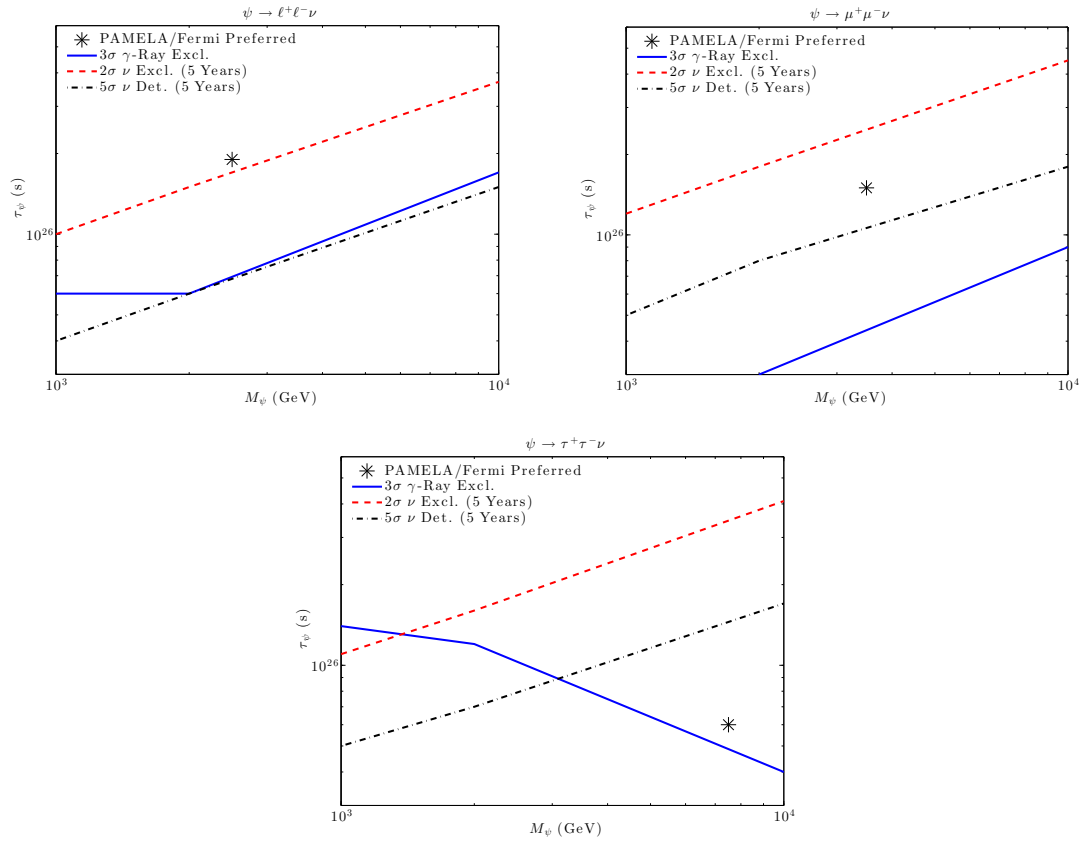
Figure 4.5: Exclusion/detection plots for some flavor-conserving decays. The exclusion/detection regions are *below* the curves. The solid line is the 3σ exclusion line from Fermi LAT gamma-ray data. The dashed line is the potential 2σ exclusion line from IceCube after 5 years of running, and the dot-dashed line is the potential 5σ discovery line from IceCube after 5 years of running. See the text for an explanation of any "kinks" that appear.
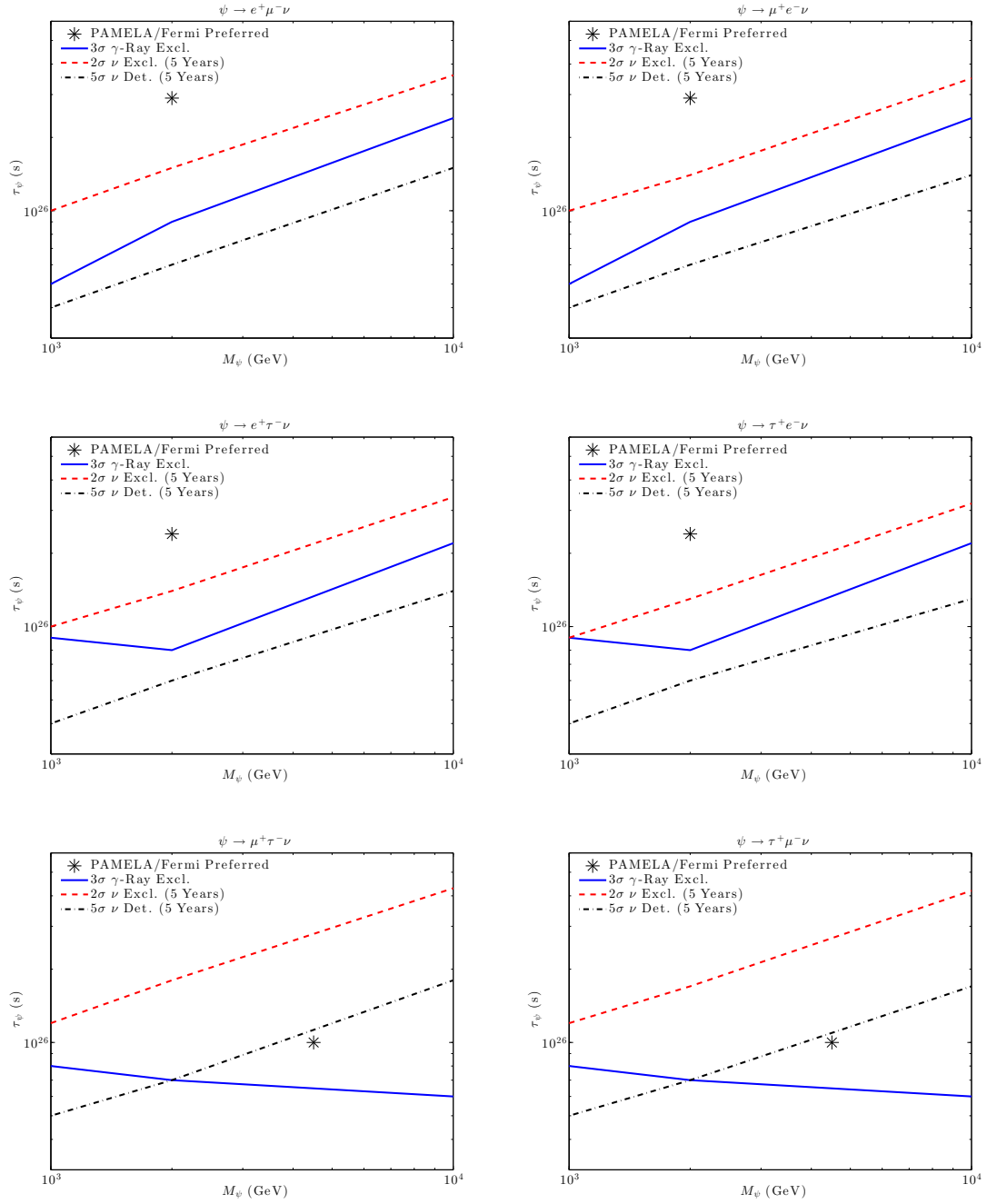
Figure 4.6: Exclusion/detection plots for some flavor-violating decays. Same as Fig. 4.5.

Chapter 5

Conclusion

We have analyzed the cosmic-ray signals of possible three-body dark-matter decays as a response to the electron-positron excess observed by the PAMELA and Fermi LAT collaborations. We assumed decays of the form $\psi \to \ell_i^+ \ell_j^- \nu$ where $\ell_i^\pm$ is a charged lepton of the ith generation and ν is a neutrino (as opposed to an antineutrino).

We showed that the $e^\pm$ energy spectra resulting from these dark-matter decays can be characterized by two parameters: ξ_+ and ξ_- with $0 \leq \xi_\pm \leq 96$. We scanned the $\xi_\pm$ parameter space and found that it is always possible to obtain good fits to the PAMELA and Fermi LAT by a suitable choice of the dark-matter mass, m_ψ, and lifetime, τ_ψ.

We also showed that the ν energy spectra resulting from these dark-matter decays can be characterized by three parameters: ξ_+, ξ_- and ξ_0. We argued that the flavor of the hard ν produced in the initial dark-matter decay is of no consequence since there is roughly equal probability that it will oscillate into any other flavor as it travels through the Milky Way Galaxy to the Earth. We then calculated the expected $\nu_\mu + \bar{\nu}_\mu$ flux from dark-matter decay and determined whether IceCube/DeepCore would be able to detect or exclude this flux after five years of running.

Finally, we computed the expected gamma-ray flux from dark-matter decays.

Since the hard ν is stable, the γ flux is characterized by ξ_+ and ξ_- only. There are two main contributions to this flux. The first comes from gamma rays produced in the dark-matter decay chain. Now, the electrons and positrons created in the decay chain can also contribute to the gamma-ray flux by undergoing inverse Compton scattering off of ambient photons. This is the second contribution to the gamma-ray flux. We computed the isotropic extragalactic gamma-ray flux due to dark-matter decays and compared it to measurements made by the Fermi LAT collaboration. We find that the flux from dark-matter decays does not conflict with the Fermi LAT data.

In conclusion, three-body dark-matter decays of the form $\psi \to \ell_i^+ \ell_j^- \nu$ constitute a possible explanation for the electron-positron excess observed by the PAMELA and Fermi LAT collaborations.

Appendix A

PYTHIA 8.1 Code

Below is a sample program for the generation of electron-positron energy spectra coming from decays involving muons. The program is written in C++ and uses the PYTHIA 8.1 package [22]. This particular program generates positron and electron spectra for the decay of an antimuon with a single-differential decay distribution that goes as E^2 (with the appropriate normalization coefficient). There is a complementary program that does the same for a decay distribution that goes as E^3. These two spectra can then be used to form linear combinations corresponding to any choice for ξ_+. The spectra of electrons and positrons due to the decay of a muon (as opposed to an antimuon) can be found by charge symmetry; in this case, the linear combinations correspond to a choice for ξ_-. Similar programs were written for the decays of positrons and antitaus and also for the energy spectra of neutrinos and photons.

```
1   //Create a dark matter particle with a given mass and allow
2         it to decay to electrons and positrons.
3   //Generate a large number of events and create a histogram
4         of electron and positron energies.
5   //Normalize this histogram to the number of events and
6         export to a text file.
7   //There is a .cmnd file which sets the center of mass energy
8          and the allowed decays.
9   //We use a Generic Resonance to simulate the dark matter
10        particle.
```

```
11
12   //The decay can have different energy spectra depending on
13            the model chosen.
14   //Since the single-differential decay distributions are
15           linear combinations of E^2 and E^3, we generate
16           electron-positron energy spectra for E^2 (Gen1) and E^3
17           (Gen2) separately. Outside of PYTHIA, one can take linear
18           combinations to get the desired energy spectra.
19
20   //We generate two energy spectra: positrons created by the
21           antilepton and electrons created by the antilepton. The
22           electrons/positrons created by the lepton can be
23           determined by symmetry.
24
25
26   #include "Pythia.h"
27   #include <fstream>
28
29   using namespace Pythia8;
30
31   //===========================================================
32
33
34   // A derived class for (e+ e- ->) GenericResonance ->
35           various final states.
36
37   class Sigma1GenRes : public Sigma1Process {
38
39   public:
40
41   // Constructor.
42   Sigma1GenRes() {}
43
44   // Evaluate sigmaHat(sHat): dummy unit cross section.
45   virtual double sigmaHat() {return 1.;}
46
47   // Select flavour. No colour or anticolour.
48   virtual void setIdColAcol() {setId( -11, 11, 999999);
49   setColAcol( 0, 0, 0, 0, 0, 0);}
50
51   // Info on the subprocess.
52   virtual string name()    const {return "GenericResonance";}
53   virtual int    code()    const {return 9001;}
54   virtual string inFlux()  const {return "ffbarSame";}
55
```

```
56   };
57
58   //==========================================================
59
60
61
62   //Set up a command for exporting arrays to text files
63   void exportToFile(double counter1[], int counterSize, string
64          filename)
65   {
66   ofstream myfile;
67   myfile.open (filename.c_str());
68   for(int i = 0; i < counterSize; i++)
69   myfile << counter1[i] << "\n";
70   myfile.close();
71   }
72
73
74   //Set the center of mass energy -- make sure to coordinate
75          with the .cmnd file
76   #define eCM 3000
77   int halfeCM = 0.5*eCM;
78
79   //Choose the number of events to generate
80   #define nEvent 2000000
81
82   //Choose the desired number to be selected
83   #define nDesired 1000000
84
85   //Choose the size of each bin (in GeV) for the electron and
86          positron histograms
87   #define binSize 0.1
88
89
90
91   int main() {
92
93   // Pythia generator.
94   Pythia pythia;
95
96   // A class to generate the fictitious resonance initial
97          state.
98   SigmaProcess* sigma1GenRes = new Sigma1GenRes();
99
100  // Hand pointer to Pythia.
```

```
101    pythia.setSigmaPtr( sigma1GenRes);
102
103    // Read in the rest of the settings and data from a
104            separate file.
105    pythia.readFile("psimu+mu-nu3000.cmnd");
106
107    // Initialization.
108    pythia.init();
109
110    // Extract settings to be used in the main program.
111    int    nList   = pythia.mode("Main:numberToList");
112    int    nShow   = pythia.mode("Main:timesToShow");
113    int    nAbort  = pythia.mode("Main:timesAllowErrors");
114
115
116    cout << " " << endl;
117    cout << " " << endl;
118
119
120
121    //Initialize the positron and electron histograms
122    //The histograms count positron and electron energies
123            between 0 GeV and halfeCM GeV with a bin size defined
124            above
125    int histSize = (halfeCM + 0.0)/binSize;
126    int posHist[histSize];
127    int elHist[histSize];
128    int muHist[histSize];
129    for (int n = 0; n < histSize; ++n) {
130    posHist[n] = 0;
131    elHist[n] = 0;
132    muHist[n] = 0;
133    }
134
135
136    //Initialize the mu+ counter and the mu+ energy spectrum vector.
137    int muCounter[histSize];
138    double Pmu[histSize];
139
140
141    //Set energy spectrum vector and mu+ counter
142    for (int n = 0; n < histSize; ++n) {
143    muCounter[n] = 0;
144    double E1 = (n + 0.0)*binSize;
145    double E2 = (n + 1)*binSize;
```

```
146   Pmu[n] = (8/(pow(eCM,3)))*(pow(E2,3) - pow(E1,3));
147   }
148
149
150   //Check that the energy spectrum vector is properly normalized
151   double PmuCheck = 0;
152   for (int i = 0; i < histSize; ++i) {
153   PmuCheck = PmuCheck + Pmu[i];
154   }
155   cout << " " << endl;
156   cout << "Check that energy spectrum is normalized:  Sum
157          of probabilities = " << PmuCheck << endl;
158   cout << " " << endl;
159   cout << " " << endl;
160
161
162   //Number of events selected to contribute to the histograms
163   int nSelected = 0;
164
165   //Initialize the number of multiple-positron events listed
166   int multipleslist = 0;
167
168
169   //Begin event loop
170   int nPace = max(1, nEvent / max(1, nShow) );
171   int iAbort = 0;
172   for (int iEvent = 0; iEvent < nEvent; ++iEvent) {
173   if (nSelected < nDesired) {
174   if (nShow > 0 && iEvent%nPace == 0)
175   cout << " Now begin event " << iEvent << endl;
176
177   //Generate events.  Quit if many failures.
178   if (!pythia.next()) {
179   if (++iAbort < nAbort) continue;
180   cout << " Event generation aborted prematurely, owing to
181          error! \n";
182   break;
183   }
184
185   //List first few events
186   if (iEvent < nList) {
187   cout << " Random Event " << iEvent + 1 << endl;
188   pythia.event.list();
189   cout << " " << endl;
190   cout << " " << endl;
```

41

```
191    cout << " " << endl;
192    cout << " " << endl;
193    }
194
195    //Initialize mu+ energy at a value not covered by the
196            energy spectrum vector;
197    //the positrons/electrons will not be counted unless this
198            value changes
199    int nEmu = (eCM + 1)/binSize;
200
201    //Initialize the mu+ number (from the event record)
202    int muNo = 0;
203
204    //Pick out the mu+ energy
205    //This is the original mu+ -- NOT any produced in the
206            subsequent shower
207    for (int i = 0; i < pythia.event.size(); ++i) {
208    if (pythia.event[i].mother1() == 5) {   //Only select
209            particles created by the Generic Resonance
210    if (pythia.event[i].id() == -13) {      //mu+
211    muNo = i;         //Record mu+ number
212    double Emu = pythia.event[i].e();
213    for (int n = 0; n < histSize; ++n) {
214    if (Emu >= (n+0.0)*binSize && Emu < (n+1)*binSize) {
215    nEmu = n;
216    }
217    }
218    }
219    }
220    }
221
222    //Determine the number of positrons produced
223    int multiplescount = 0;
224    for (int i = 0; i < pythia.event.size(); ++i) {
225    if (pythia.event[i].isFinal() && pythia.event[i].id() == -11) {
226    multiplescount = multiplescount + 1;
227    }
228    }
229    int nMultiple = 6;
230    int listq = 0;
231    if (multiplescount == nMultiple && multipleslist < 1) {
232    multipleslist = multipleslist + 1;
233    pythia.event.list();
234    listq = 1;
235    }
```

```
236
237
238   //Pick out positron energy -- but only if the mu+ energy
239          was changed to an allowed value
240   if (nEmu < (eCM + 1)/binSize) {
241   if (muCounter[nEmu] < ((nDesired + 0.0)*Pmu[nEmu] - 0.5)) {
242   muHist[nEmu] = muHist[nEmu] + 1;
243   nSelected = nSelected + 1;
244   for (int i = 0; i < pythia.event.size(); ++i) {
245   if (pythia.event[i].isFinal()) {        //only consider stable
246          particles
247   double eI = pythia.event[i].e();
248   if (pythia.event[i].id() == -11) {      //e+
249   int q = i; //Trace mothers until muNo
250   for (int j = 0; j < pythia.event.size(); ++j) {
251   if (q > muNo) {
252   q = pythia.event.motherList(q)[0];
253   }
254   }
255   if (multiplescount == nMultiple && listq == 1) {
256   cout << " Particle " << i << " originated from particle "
257          << q << endl;
258   }
259   if (q == muNo) {        //Only consider positrons created by
260          the mu+
261   for (int n = 0; n < histSize; ++n) {
262   //record positron energy in appropriate bin
263   if (eI >= (n + 0.0)*binSize && eI < (n + 1)*binSize) {
264   posHist[n] = posHist[n] + 1;
265   }
266   }
267   }
268   }
269   if (pythia.event[i].id() == 11) {       //e-
270   int q = i; //Trace mothers until muNo
271   for (int j = 0; j < pythia.event.size(); ++j) {
272   if (q > muNo) {
273   q = pythia.event.motherList(q)[0];
274   }
275   }
276   if (multiplescount == nMultiple && listq == 1) {
277   cout << " Particle " << i << " originated from particle "
278          << q << endl;
279   }
280   if (q == muNo) {        //Only consider electrons created by
```

```
281          the mu+
282   for (int n = 0; n < histSize; ++n) {
283   //record electron energy in appropriate bin
284   if (eI >= (n + 0.0)*binSize && eI < (n + 1)*binSize) {
285   elHist[n] = elHist[n] + 1;
286   }
287   }
288   }
289   }
290   }
291   }
292   }
293   }
294
295   //Enter the event in the muCounter matrix
296   muCounter[nEmu] = muCounter[nEmu] + 1;
297   }
298   }
299
300
301   //Print a small section of the histogram
302   int nSampleMin = 0.0*(halfeCM + 0.0);
303   int nSampleMax = nSampleMin + 5;
304   cout << " " << endl;
305   cout << " " << endl;
306   cout << "----Sample Section of Histogram (" << nSampleMin
307          << " GeV <= E <= " << nSampleMax << " GeV)" << endl;
308   cout << " " << endl;
309   cout << left << setw(15) << "Energy (GeV)" << "No. e+" << endl;
310   cout << " " << endl;
311   for (int n = (nSampleMin + 0.0)/binSize; n < (nSampleMax +
312          0.0)/binSize; ++n) {
313   cout << left << setw(17) << (n + 0.5)*binSize << eHist[n]
314          << endl;
315   }
316
317
318   //Check that each muCounter entry is maxed out
319   int muCheck = 0;
320   for (int n = 0; n < histSize; ++n) {
321   if (muCounter[n] <= nDesired*Pmu[n] - 0.5) {
322   muCheck = muCheck + 1;
323   }
324   }
325
```

```
326
327    //Print the number of generated and selected events
328    cout << " " << endl;
329    cout << " " << endl;
330    cout << " Number of Events Generated: " << nEvent << endl;
331    cout << " Number of Events Desired: " << nDesired << endl;
332    cout << " Number of Events Selected: " << nSelected << endl;
333    cout << " Number of muCounter entries NOT at maximum capacity:
334           " << muCheck << "/" << histSize << endl;
335
336
337    //Normalize e histograms to the bin size and the number of
338           selected events
339    double elHistNormalized[histSize];
340    double posHistNormalized[histSize];
341    for (int n = 0; n < histSize; ++n) {
342    elHistNormalized[n] = (elHist[n] + 0.0)/((nDesired +
343           0.0)*binSize);
344    posHistNormalized[n] = (posHist[n] + 0.0)/((nDesired +
345           0.0)*binSize);
346    }
347
348
349    //Send normalized histograms to external text files
350    exportToFile(posHistNormalized, histSize, "mu+Pos3000Gen1.txt");
351    exportToFile(elHistNormalized, histSize, "mu+El3000Gen1.txt");
352
353
354    return 0;
355    }
```

Bibliography

[1] O. Adriani *et al.* [PAMELA Collaboration], Nature **458**, 607-609 (2009). [arXiv:0810.4995 [astro-ph]].

[2] A. A. Abdo *et al.* [The Fermi LAT Collaboration], Phys. Rev. Lett. **102**, 181101 (2009). [arXiv:0905.0025 [astro-ph.HE]].

[3] F. Aharonian *et al.* [H.E.S.S. Collaboration], Astron. Astrophys. **508**, 561 (2009). [arXiv:0905.0105 [astro-ph.HE]].

[4] D. Hooper, P. Blasi, P. D. Serpico, JCAP **0901**, 025 (2009). [arXiv:0810.1527 [astro-ph]].

[5] H. Yuksel, M. D. Kistler, T. Stanev, Phys. Rev. Lett. **103**, 051101 (2009). [arXiv:0810.2784 [astro-ph]].

[6] I. Cholis, L. Goodenough, D. Hooper, M. Simet, N. Weiner, Phys. Rev. **D80**, 123511 (2009). [arXiv:0809.1683 [hep-ph]].

[7] M. Cirelli, M. Kadastik, M. Raidal, A. Strumia, Nucl. Phys. **B813**, 1-21 (2009). [arXiv:0809.2409 [hep-ph]].

[8] E. Nardi, F. Sannino, A. Strumia, JCAP **0901**, 043 (2009). [arXiv:0811.4153 [hep-ph]].

[9] Y. Z. Fan, B. Zhang and J. Chang, Int. J. Mod. Phys. D **19**, 2011 (2010) [arXiv:1008.4646 [astro-ph.HE]].

[10] D. E. Kaplan, M. A. Luty, K. M. Zurek, Phys. Rev. **D79**, 115016 (2009). [arXiv:0901.4117 [hep-ph]].

[11] M. R. Buckley, L. Randall, [arXiv:1009.0270 [hep-ph]].

[12] J. Shelton, K. M. Zurek, Phys. Rev. **D82**, 123512 (2010). [arXiv:1008.1997 [hep-ph]].

[13] A. Falkowski, J. T. Ruderman, T. Volansky, JHEP **1105**, 106 (2011). [arXiv:1101.4936 [hep-ph]].

[14] M. T. Frandsen, I. Masina, F. Sannino, Phys. Rev. **D83**, 127301 (2011). [arXiv:1011.0013 [hep-ph]].

[15] S. Chang, L. Goodenough, [arXiv:1105.3976 [hep-ph]].

[16] I. Masina, F. Sannino, [arXiv:1106.3353 [hep-ph]].

[17] J. T. Ruderman, T. Volansky, [arXiv:0907.4373 [hep-ph]]; A. Falkowski, J. Juknevich, J. Shelton, [arXiv:0908.1790 [hep-ph]].

[18] A. Kounine, [arXiv:1009.5349 [astro-ph.HE]].

[19] H. -C. Cheng, W. -C. Huang, I. Low, A. Menon, JHEP **1103**, 019 (2011). [arXiv:1012.5300 [hep-ph]].

[20] E. D. Commins, P. H. Bucksbaum, "Weak Interactions Of Leptons And Quarks," Cambridge University Press, (1983) 484p.

[21] R. Mertig, M. Bohm, A. Denner, Comput. Phys. Commun. **64**, 345-359 (1991).

[22] T. Sjostrand, S. Mrenna, P. Z. Skands, JHEP **0605**, 026 (2006). [hep-ph/0603175].

[23] J. F. Navarro, C. S. Frenk, S. D. M. White, Astrophys. J. **462**, 563-575 (1996). [astro-ph/9508025].

[24] D. Hooper, J. Silk, Phys. Rev. **D71**, 083503 (2005). [hep-ph/0409104]; E. A. Baltz, J. Edsjo, Phys. Rev. **D59**, 023511 (1998). [astro-ph/9808243].

[25] T. Delahaye, R. Lineros, F. Donato, N. Fornengo, P. Salati, Phys. Rev. **D77**, 063527 (2008). [arXiv:0712.2312 [astro-ph]]; F. Donato, N. Fornengo, D. Maurin, P. Salati, Phys. Rev. **D69**, 063501 (2004). [astro-ph/0306207].

[26] A. Ibarra, D. Tran, JCAP **0807**, 002 (2008). [arXiv:0804.4596 [astro-ph]].

[27] D. Grasso *et al.* [FERMI-LAT Collaboration], Astropart. Phys. **32**, 140-151 (2009). [arXiv:0905.0636 [astro-ph.HE]].

[28] A. Ibarra, D. Tran, C. Weniger, JCAP **1001**, 009 (2010). [arXiv:0906.1571 [hep-ph]].

[29] R. Gandhi, C. Quigg, M. H. Reno, I. Sarcevic, Phys. Rev. **D58**, 093009 (1998). [hep-ph/9807264].

[30] E. Resconi, f. t. I. Collaboration, Nucl. Instrum. Meth. **A602**, 7-13 (2009). [arXiv:0807.3891 [astro-ph]].

[31] J. G. Learned, K. Mannheim, Ann. Rev. Nucl. Part. Sci. **50**, 679-749 (2000).

[32] M. Honda, T. Kajita, K. Kasahara, S. Midorikawa and T. Sanuki, Phys. Rev. D **75**, 043006 (2007) [astro-ph/0611418].

[33] C. -R. Chen, S. K. Mandal, F. Takahashi, JCAP **1001**, 023 (2010). [arXiv:0910.2639 [hep-ph]].

[34] A. Ibarra, D. Tran, Phys. Rev. Lett. **100**, 061301 (2008). [arXiv:0709.4593 [astro-ph]].

[35] M. R. Buckley, K. Freese, D. Hooper, D. Spolyar, H. Murayama, Phys. Rev. **D81**, 016006 (2010). [arXiv:0907.2385 [astro-ph.HE]].

[36] S. K. Mandal, M. R. Buckley, K. Freese, D. Spolyar, H. Murayama, Phys. Rev. **D81**, 043508 (2010). [arXiv:0911.5188 [hep-ph]].

[37] L. Covi, M. Grefe, A. Ibarra, D. Tran, JCAP **1004**, 017 (2010). [arXiv:0912.3521 [hep-ph]].

[38] M. Cirelli, P. Panci, P. D. Serpico, Nucl. Phys. **B840**, 284-303 (2010). [arXiv:0912.0663 [astro-ph.CO]].

[39] A. A. Abdo *et al.* [The Fermi-LAT Collaboration], Phys. Rev. Lett. **104**, 101101 (2010) [arXiv:1002.3603 [astro-ph.HE]].

[40] P. Meade, M. Papucci, A. Strumia and T. Volansky, Nucl. Phys. B **831**, 178 (2010) [arXiv:0905.0480 [hep-ph]].

[41] T. A. Porter and A. W. Strong, astro-ph/0507119.

[42] M. Cirelli, G. Corcella, A. Hektor, G. Hutsi, M. Kadastik, P. Panci, M. Raidal and F. Sala *et al.*, JCAP **1103**, 051 (2011) [arXiv:1012.4515 [hep-ph]].

[43] M. Cirelli, F. Iocco and P. Panci, JCAP **0910**, 009 (2009) [arXiv:0907.0719 [astro-ph.CO]].